RSC Advances

PAPER

View Article Online
View Journal | View Issue

Cite this: *RSC Adv.*, 2022, **12**, 35943

Carbon nanotube–titanium dioxide nanocomposite support for improved activity and stability of an iridium catalyst toward the oxygen evolution reaction†

Eom Ji Kim, Ki hyun Kim, Junu Bak, KwangHo Lee and EunAe Cho *

Received 11th August 2022
Accepted 16th November 2022

DOI: 10.1039/d2ra05027g

rsc.li/rsc-advances

In order to improve the electrocatalytic activity and stability of an iridium (Ir) nanoparticle catalyst toward the oxygen evolution reaction (OER) in acidic electrolyte, carbon nanotube and titanium dioxide nanocomposites (CNT@TiO_2) are presented as a high-performance support. TiO_2 was synthesized on CNTs by using a novel layer-by-layer solution coating method that mimics atomic layer deposition (ALD) but is cost-effective and scalable. In the nanocomposites, CNTs serve as the electron pathways and the surface TiO_2 layers protect CNTs from corrosion under the harsh OER conditions. Thus, CNT@TiO_2 demonstrates excellent corrosion resistance as well as a high electrical conductivity (1.6 ± 0.2 S cm^{-1}) comparable to that of Vulcan carbon (1.4 S cm^{-1}). The interaction between Ir and TiO_2 promotes the formation of Ir(III) species, thereby enhancing the OER activity and stability of the Ir nanoparticle catalyst. Compared to commercial carbon-supported Ir (Ir/C) and Ir black catalysts, CNT@TiO_2-supported Ir exhibits superior OER activity and stability.

1. Introduction

Renewable energy is indispensable for dealing with upcoming climate change issues. Accordingly, energy storage technologies have become crucial topics in the energy industry to address the intermittency of renewable electricity. Water electrolysis that converts electricity into hydrogen is considered as a promising candidate to store surplus renewable electricity. In particular, polymer electrolyte water electrolysis (PEMWE) thanks to their wide load range and fast response to be directly connected to renewable electricity.[1,2] One of the main huddles of commercialization of the PEMWE is the usage of large amount of precious metal catalysts, particularly iridium (Ir), to overcome the sluggish oxygen evolution reaction (OER) at the anode.[3] To reduce the amount of Ir catalyst usage, Ir has been alloyed or shape-controlled, exhibiting enhanced OER activity.[4,5] However, stability of those catalysts is an obstacle to applications. As an alternative, support can be introduced since support not only distributes but also stabilizes the small catalyst nanoparticles, resulting in improved catalyst performance. In polymer electrolyte membrane fuel cell (PEMFC), carbon black has been widely used as a support for platinum nanoparticle catalyst.[6] However, at the high anode potentials of PEMWE, carbon black is easily corroded and cannot be utilized as a support. Thus, electrically-conductive and corrosion-resistant support materials should be developed for Ir nanoparticle catalyst.[7]

Firstly, carbon materials with higher crystallinity have been proposed as support since they have better corrosion resistance than carbon black.[8] For instance, multiwall-carbon nanotube (MWCNT)-supported IrO_2 has presented high OER activity in acidic electrolytes.[9–11] Although MWCNT has better corrosion resistance than carbon black,[8,12,13] it is also corroded at the high anode potentials and durability of MWCNT-supported IrO_2 needs to be improved. Secondly, metal oxides such as titanium dioxide (TiO_2) and tin dioxide (SnO_2) have been explored with an advantage of excellent corrosion resistance under acidic and high potential conditions.[14–20] However, they have an obvious drawback of extremely low electrical conductivity,[21–23] that obstructs electron transfer during the OER and significantly increases the overpotential.[17] To overcome the problem, metal oxides have been doped with various dopants such as niobium and vanadium.[24,25] However, dopants-related degradation of the oxide supports has been reported particularly for doped SnO_2.[26]

In this study, we present CNT and TiO_2 nanocomposites (CNT@TiO_2) that combine the electrical conductivity of CNT with corrosion resistance of TiO_2 as a support for Ir nanoparticles. TiO_2 was synthesized on CNTs using a novel layer-by-layer solution coating method, that mimics atomic layer deposition (ALD)[27] but is cost-effective and scalable. Ir nanoparticles supported on CNT@TiO_2 nanocomposite (Ir/CNT@TiO_2) demonstrate superior OER activity and stability to commercial

Department of Materials Science and Engineering, Korea Advanced Institute of Science and Technology (KAIST), 291 Daehak-ro, Yuseong-gu, Daejeon 34141, Republic of Korea. E-mail: eacho@kaist.ac.kr

† Electronic supplementary information (ESI) available. See DOI: https://doi.org/10.1039/d2ra05027g

Ir black and carbon-supported Ir and catalysts. As a descriptor of OER activity, oxidation states of Ir were examined by using X-ray photoelectron spectroscopy (XPS).

2. Experimental

2.1. Synthesis of CNT@TiO_2 nanocomposites

To prepare CNT and TiO_2 nanocomposites (CNT@TiO_2), multiwall carbon nanotubes purchased from Sigma Aldrich were immersed in a solution of nitric acid and sulfuric acid at room temperature for 12 hours. TiO_2 was synthesized on the acid-treated CNTs using a solution-based layer-by-layer coating method presented in Fig. S1.† 2 mL of titanium tetra isopropoxide (TTIP) were dissolved in 40 mL of isopropyl alcohol (IPA). Then, 40 mg of the acid-treated CNTs were added to the solution and sonicated for 30 min. The prepared mixture was kept at 80 °C for 2 hours for the adsorption of TTIP on the acid-treated CNTs and filtered. The collected powder was washed with ethanol. Then, DI water was dropped onto the powder for hydrolysis of TTIP adsorbed on CNT. The products were collected and dried in a convection oven at 60 °C for 3 hours. The adsorption and hydrolysis processes were alternately repeated 2, 4, 6 and 8 times to obtain corresponding number of TiO_2 layers on CNT. Then, the products were heated at 350 °C in air for 2 hours for calcination.

2.2. Synthesis of Ir/CNT and Ir/CNT@TiO_2

Ir nanoparticles were synthesized on the acid-treated CNT and the prepared CNT@TiO_2 and using a polyol reduction method.[28] To load 40 wt% of Ir, 80 mg of support and 134 mg of potassium hexachloroiridiate(IV) (K_2IrCl_6) were mixed with 50 mL ethylene glycol and sonicated for 60 min. The solution pH was adjusted to 10 using 1 M potassium hydroxide solution. The prepared mixture was kept at 170 °C for 3 h under argon bubbling and cooled to room temperature. The precipitates were filtered, washed with DI water, and dried in a convection oven at 60 °C overnight.

2.3. Materials characterization

The morphology of the samples was observed using a Hitachi SU8230 scanning electron microscope (SEM). Crystal structure was identified by X-ray diffraction (XRD) using a Rigaku Dmax-2500 with Cu Kα radiation. Transmission electron microscopy (TEM) images were obtained from a Tecnai G2 F20 S-Twin. High-angle annular dark-field (HAADF) images and energy dispersive spectroscopy (EDS) mapping images were taken using a Titan cubed G2 under 200 kV. The chemical composition of the prepared samples was obtained by inductively coupled plasma mass spectroscopy (ICP-MS). For ICP-MS, the prepared Ir/CNT@TiO_2 samples were pre-treated in a mixed solution of 70% HNO_3 and 35% HCl (7 : 3 in vol%) at 200 °C for 30 minutes in a microwave. Electrical conductivity was measured using a home-made apparatus.[29] For the measurement, powder samples were pressed to form cylindrical pellets and conductivity was obtained with applying a compressive load to the pellets.

X-ray photoelectron spectroscopy (XPS) was conducted using a ThermoFisher Scientific MXP10. For the measurement, catalyst-coated-carbon papers were fabricated. The catalyst inks were prepared by mixing 3 mg of catalyst powder and 20 μL of a Nafion solution (5 wt%, 1100 EW, Dupont) were dispersed in D.I. water and IPA and then sonicated for 30 min. The prepared catalyst ink was coated on a carbon paper and dried at room temperature for 30 min. The prepared catalyst-coated-carbon papers were activated in 0.05 M H_2SO_4 solution by conducting potential cycling between 1.0 and 1.8 V_{RHE} for 3 cycles at a scan rate of 5 mV s^{-1} before XPS measurement. Binding energy values were calibrated with respect to the C 1s position (C sp^2: 284.2 eV).

2.4. Electrochemical measurements

Electrocatalytic activity and stability were evaluated using a potentiostat (Pine Instruments) with a standard three-electrode electrochemical cell. Pt mesh and a saturated calomel electrode (SCE) were used as counter electrode and reference electrode, respectively. All potentials were converted to that of a reversible hydrogen electrode (RHE). The catalyst ink prepared to fabricated the catalyst-coated-carbon papers. The prepared catalyst ink was coated on the surface of a glassy carbon electrode (GCE) and dried at room temperature for 5 min in a vacuum cell. Ir loading amount on GCE was 10 μg_{Ir} cm^{-2}. OER polarization curves were measured in an Ar-saturated 0.05 M H_2SO_4 solution at a scan rate of 5 mV s^{-1} with a rotating speed of 2500 rpm. To estimate the stability of the catalysts, chronopotentiometry was conducted at 10 mA cm^{-2} with 2500 rpm. Electrochemical impedance spectroscopy was conducted at 1.51 V_{RHE} from 10 mHz to 100 kHz.

3. Results & discussion

To prepare CNT and TiO_2 nanocomposites, multiwall CNTs were acid treated and then coated with TiO_2 through three steps; adsorption of Ti precursor (titanium tetra isopropoxide, TTIP) on CNTs, hydrolysis of TTIP to $Ti(OH)_x$, and calcination of $Ti(OH)_x$ to TiO_2 (Fig. S1†). As-purchased and acid-treated CNTs (Fig. S1†) exhibit approximately the same one-dimensional structure with diameter of 50–60 nm, revealing that the acid treatment has negligible effects on the morphology of CNTs. However, without the acid treatment, TiO_2 was not formed on CNTs, implying that the acid treatment modifies surface properties of CNTs for TTIP adsorption.[30] The acid-treated multiwall CNTs are simply denoted as CNTs hereafter. Aiming at forming 2, 4, 6 and 8 layers of TiO_2 on CNTs (denoted as CNT@TiO_2-n L, n = 2, 4, 6 and 8), adsorption and hydrolysis steps were alternately repeated 2, 4, 6, and 8 times before calcination. To examine the effects of TiO_2 coating on the pore structure, N_2-adsorption–desorption isotherms were measured for CNT and CNT@TiO_2-6 L (Fig. S2†). Brunauer–Emmet–Teller (BET) surface areas of CNT and CNT@TiO_2-6 L were calculated and found to be 166.1 and 151.9 m^2 g^{-1}, respectively. Pore size distributions show that the average pore sizes of CNT and CNT@TiO_2-6 L are 17.8 and 10.9 nm, respectively. The

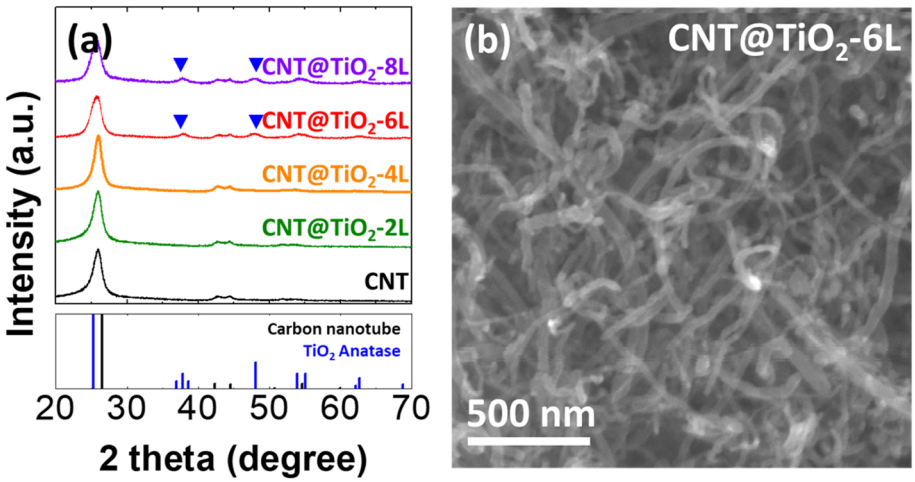

Fig. 1 (a) XRD patterns of acid-treated CNT and CNT@TiO_2-*n* L nanocomposites (*n* = 2, 4, 6 and 8). (b) SEM image of CNT@TiO_2-6 L nanocomposites.

decreases in BET surface area and average pore size can be related to the coating heavier TiO_2 layer to CNT.

Fig. 1a demonstrates XRD patterns of CNT and CNT@TiO_2-*n* L nanocomposites. CNT, CNT@TiO_2-2 L, and CNT@TiO_2-4 L exhibit XRD peaks from CNT whereas CNT@TiO_2-6 L and CNT@TiO_2-8 L demonstrate XRD peaks corresponding to anatase TiO_2 in addition to the CNT peaks. The absence of the TiO_2-related peaks from the XRD patterns of CNT@TiO_2-2 L and CNT@TiO_2-4 L could be attributed to the low contents of TiO_2. CNT@TiO_2-*n* L nanocomposites (Fig. 1b and S4†) show one-dimensional structure similar to CNTs (Fig. S3†) without precipitates or segregated particles. While the acid-treated CNTs have average wall thickness of approximately 13 nm, CNT@TiO_2-2 L and CNT@TiO_2-4 L demonstrate thicker walls with average thickness of approximately 14 and 16 nm, respectively (Fig. S5†). Ti compositions in CNT@TiO_2-2 L and CNT@TiO_2-4 L are 1.1 and 3.4 at%, respectively (Table S1†). These results demonstrate that TiO_2 was mostly coated on CNTs

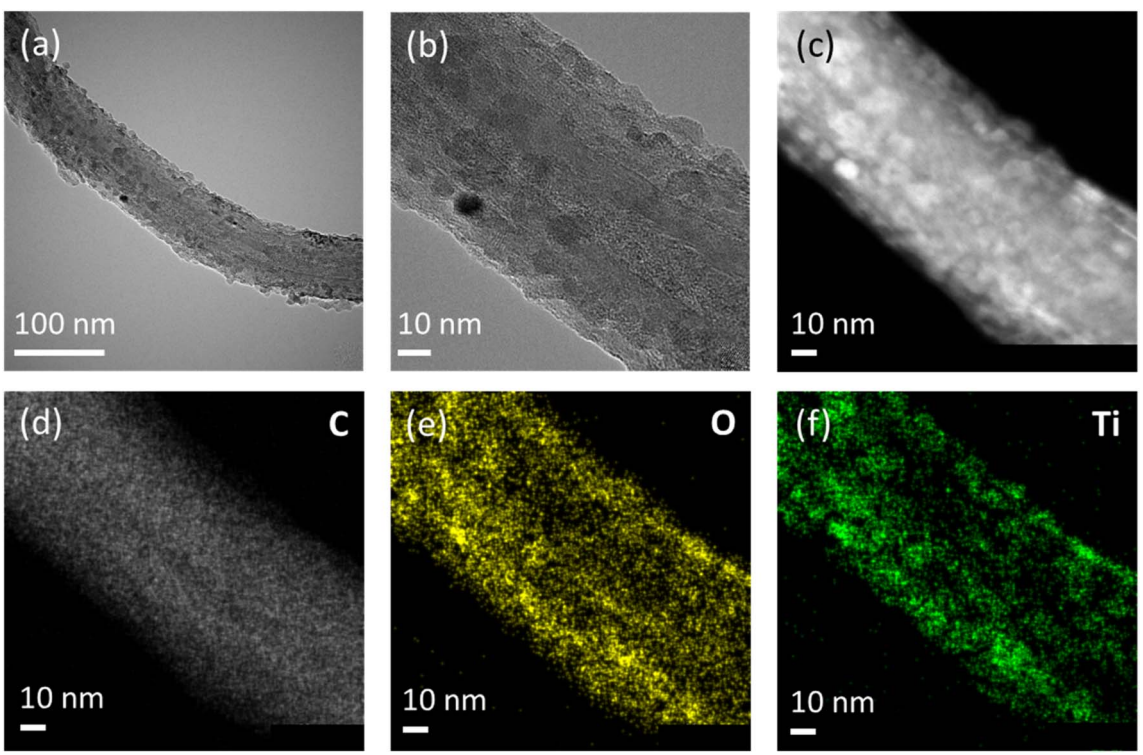

Fig. 2 (a) and (b) TEM images, (c) HAADF STEM image and EDS elemental mapping for (d) carbon, (e) oxygen and (f) titanium of CNT@TiO_2-6 L nanocomposites.

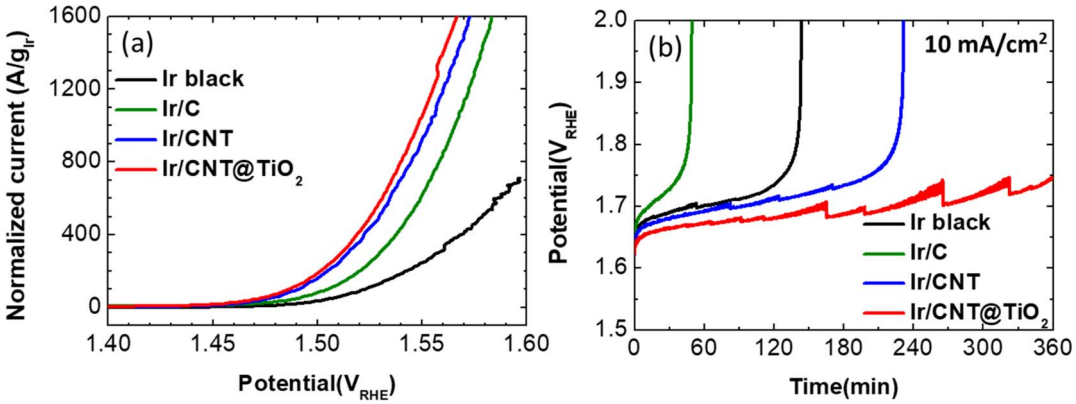

Fig. 3 (a) OER polarization curves normalized by Ir loading amounts on RDE and (b) durability measurement at 10 mA cm^{-2} in Ar-saturated 0.05 M H_2SO_4 electrolyte for Ir black, Ir/C, Ir/CNT and Ir/CNT@TiO_2.

rather than formed as a separate phase in those samples and with repeating the adsorption and hydrolysis steps, thicker TiO_2 layers were formed. On the other hand, CNT@TiO_2-6 L (Fig. 2) and CNT@TiO_2-8 L (Fig. S5d†) have similar wall thickness to that of CNT@TiO_2-4 L (approximately 16 nm) and Ti compositions of 5.3 and 5.5 at%, respectively. In particular, they demonstrate a large number of TiO_2 nanoparticles well-dispersed on the TiO_2-coated CNTs. Thus, it can be inferred that, using the layer-by-layer solution method proposed in this study, TiO_2 was coated on CNTs up to a certain thickness (about 3 nm in this study) and excess TiO_2 was formed as nanoparticles. TEM and elemental mapping images (Fig. 2 and S5d†) support formation of crystalline TiO_2 nanoparticles on CNT@TiO_2-6 L and CNT@TiO_2-8 L, observed in the XRD patterns (Fig. 1a).

To evaluate performance of the prepared supports, Ir nanoparticles were synthesized on CNT (Ir/CNT) and CNT@TiO_2-*n* L with Ir contents of about 40 wt% (Ir/CNT@TiO_2-*n* L, Table S2†). The OER activity of the prepared Ir/CNT and Ir/CNT@TiO_2-*n* L catalysts was evaluated by measuring polarization curves in an Ar-saturated 0.05 M H_2SO_4 solution at a scan rate of 5 mV s^{-1}, in comparison to commercial Ir black and Ir/C (Fig. 4a and S5†). The measured polarization curves were *iR*-corrected. The loading amounts of Ir on the rotating disk electrode (RDE) were fixed at 10 μg_{Ir} cm^{-2}. Exceptively, Ir black was coated on the RDE with loading amount of 37.5 μg_{Ir} cm^{-2} to maintain the catalyst film quality. Among the prepared Ir/CNT@TiO_2-*n* L samples, Ir/CNT@TiO_2-6 L exhibited slightly higher OER activity than the others (Fig. S6†). Accordingly, CNT@TiO_2-6 L was investigated as a representative support and denoted simply as CNT@TiO_2 hereafter. Considering the Ir loading amounts, the OER polarization curves were normalized by Ir mass in Fig. 4a. The mass activity at 1.55 V_{RHE} for the Ir black, Ir/C, Ir/CNT, and Ir/CNT@TiO_2 were found to be 247, 616, 927, and 1055 A g_{Ir}^{-1}, respectively. Compared to Ir black, the supported catalysts exhibit higher mass activity, that can be associated with the well distribution of Ir nanoparticles and efficient utilization of Ir catalyst. Among the supported catalysts, Ir/CNT@TiO_2 presents the highest mass activity. Compared to the previously-reported oxide-supported Ir-based catalysts, Ir/CNT@TiO_2 demonstrates excellent OER activity, as summarized in Table S3.†

Tafel slopes for Ir black, Ir/C, Ir/CNT, and Ir/CNT@TiO_2 were found to be 48, 50, 49, and 50 mV dec^{-1}, respectively (Fig. S7a†), reflecting similar OER mechanisms on all of the prepared sample. Charge transfer resistances of the supported catalysts estimated from Nyquist plots (Fig. S7b†) were 500, 370 and 240 ohm for Ir/C, Ir/CNT, and Ir/CNT@TiO_2, respectively, in accordance with the mass activity. Due to the higher Ir loading for Ir black, it is not suitable to compare the charge transfer resistance of Ir black to those of supported catalysts.

Stability of the prepared catalysts was evaluated by conducting chronopotentiometry at a current density of 10 mA cm^{-2}, which was selected as an accelerated stability test (AST) condition based on the chronopotentiometry outcomes collected for Ir black at 1, 5, and 10 mA cm^{-2} (Fig. S8†). As shown in Fig. 3b, potentials of Ir black, Ir/C and Ir/CNT increase gradually and abruptly increase to 2.0 V_{RHE} at 140, 50 and 235 min, respectively. On the other hand, Ir/CNT@TiO_2 demonstrates potentials lower than 1.75 V during 360 min (the saw-toothed potentials is associated with the generation and removal of oxygen gas bubbles). Ir/C shows inferior stability to Ir black despite a better OER performance. These outcomes reflect that carbon black easily corroded under the OER condition and the carbon corrosion has crucial effects on the stability of the supported catalyst.[7] The better stability of Ir/CNT than Ir black and Ir/C reveals that CNT has an improved corrosion resistance than black carbon. Furthermore, Ir/CNT@TiO_2 shows the best durability superior to Ir/CNT.

As a support for Ir catalyst, TiO_2 has been known to demonstrate the poor performance due to the extremely low electrical conductivity.[17] However, Ir/CNT@TiO_2 exhibits excellent OER performance and stability compared to Ir black, Ir/C and Ir/CNT. In that respect, electrical conductivity of CNTs and CNT@TiO_2 was measured and found to be 3.2 and 1.6 ± 0.2 S cm^{-1}, respectively, using the previously-reported method.[29] Even though lower than that of CNT, electrical conductivity of CNT@TiO_2 is significantly higher than that of TiO_2 nanoparticles ($\sim 10^{-6}$ S cm^{-1}) and even comparable with that of Vulcan carbon (1.4 S cm^{-1}), one of the most widely-used

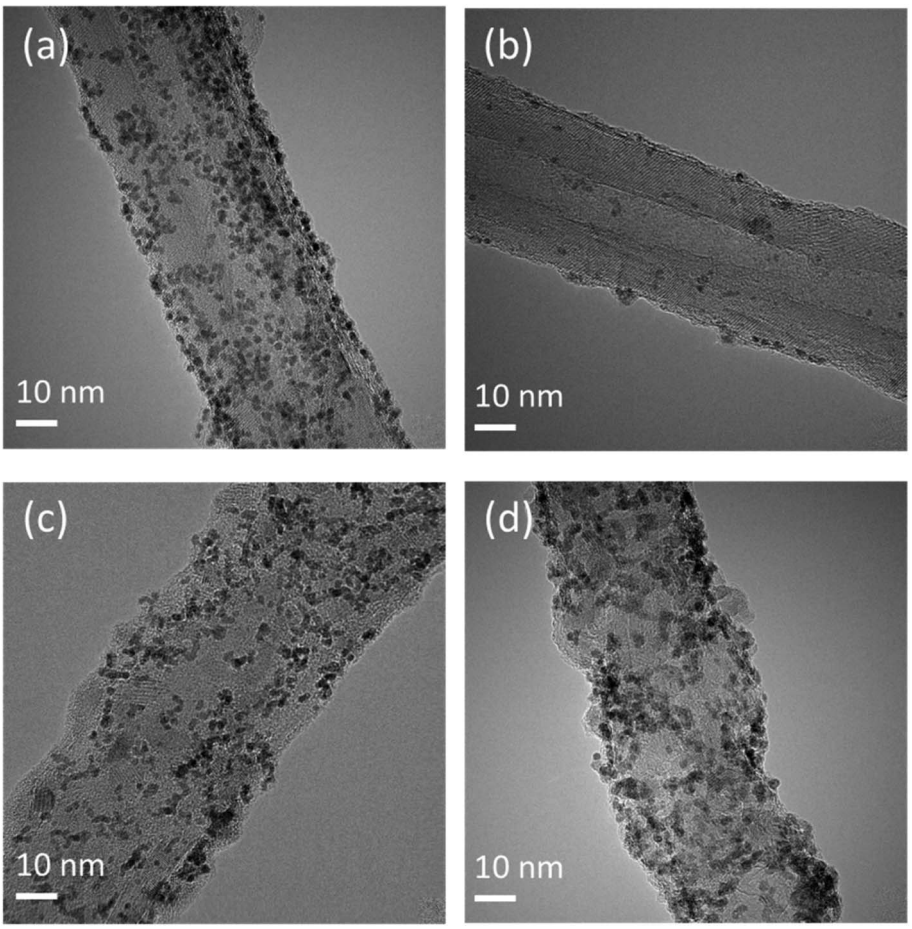

Fig. 4 TEM images of Ir nanoparticles of (a), (b) the Ir/CNT catalyst and (c), (d) the Ir/CNT@TiO_2 catalyst (a), (c) before and (b), (d) after the durability test.

support materials.[29] These results demonstrate that CNT in CNT@TiO_2 nanocomposite effectively contributes to the formation of the electron-conduction paths, enabling CNT@TiO_2 to serve as a support.

Fig. 4a and c illustrate that Ir/CNT and Ir/CNT@TiO_2 have similar sizes and distributions of Ir nanoparticles (Fig. S9–S11†), with average particle sizes of 1.61 and 1.64 nm, respectively. However, Ir/CNT@TiO_2 display higher OER activity than Ir/CNT despite lower electrical conductivity. These outcomes imply that the CNT@TiO_2 nanocomposites support, particularly TiO_2, affects electrocatalytic activity of Ir. The electronic structure of Ir is considered a crucial factor determining the catalytic performance of the OER. In particular, iridium hydroxo surface species (Ir–OH) has higher intrinsic activity toward the OER than iridium oxide surface species.[31] Since the Ir(III) species is known to be related to Ir–OH, composition of Ir(III) has been proposed as an activity descriptor for the OER.[32] Furthermore, it has been reported that the electronic structure can be modulated through interaction between Ir and oxide support.[7,29] Effects of TiO_2 on the electronic structure of Ir were investigated. XPS spectra in the Ir 4f region of Ir/CNT and Ir/CNT@TiO_2 (Fig. 5) display presence of the Ir(0), Ir(III), and Ir(IV) species.[33] In Ir/CNT, Ir species is composed of approximately 14% Ir(0), 22% Ir(III), and 64% Ir(IV) (Fig. S12†). Ir/CNT@TiO_2 presents corresponding compositions of 15, 36, and 49%. The higher composition of Ir(III) species in Ir/CNT@TiO_2 demonstrates that TiO_2 promotes the formation of Ir(III) species,[14,29] thereby enhancing the OER activity.

In addition to the improvement of the OER activity, the strong interaction between Ir and TiO_2 could affect stability of Ir catalyst.[34] To examine effects of TiO_2 on the degradation of Ir nanoparticles, Ir/CNT and Ir/CNT@TiO_2 were exposed to the AST condition of 10 mA cm^{-2} for ten hours and then observed using TEM and EDS (Fig. 4b, d, S9 and S10†). During the AST, Ir nanoparticles were substantially lost from Ir/CNT, whereas most of Ir nanoparticles were well preserved in Ir/CNT@TiO_2. In addition, the average Ir particle size of Ir/CNT was reduced to 1.49 nm (Fig. S11†), whereas that of Ir/CNT@TiO_2 was kept similar (1.68 nm, Fig. S11†). These results support that the strong interaction between Ir and TiO_2 significantly suppressed dissolution and loss of Ir nanoparticles,[14,34] thereby improving stability of Ir nanoparticle catalyst. The loss of Ir nanoparticles is known as the main origin of catalyst degradation during the OER. The enhanced stability of the Ir/CNT@TiO_2 catalyst can be attributed to (1) the higher corrosion resistance of the TiO_2 layers on CNT than that of the carbon support under OER conditions and (2) the strong interaction between Ir and metal-oxide support. These

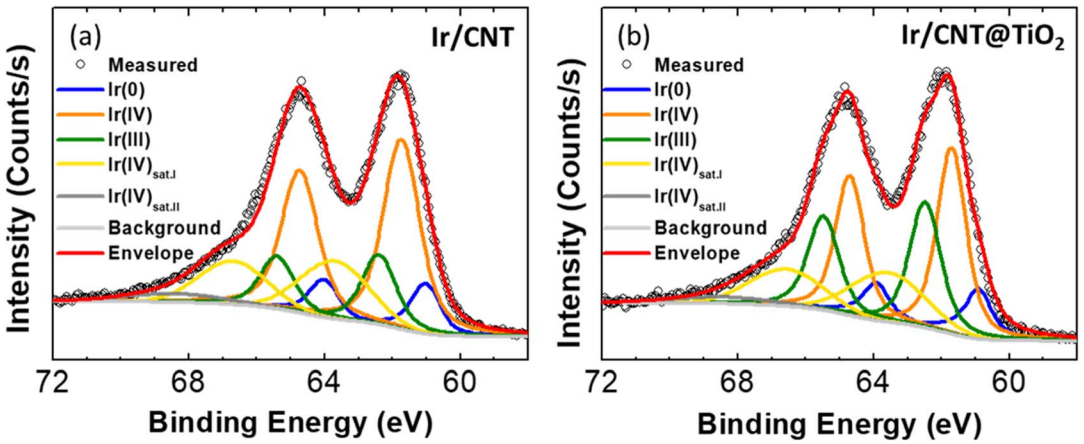

Fig. 5 XPS Ir 4f spectra of (a) Ir/CNT and (b) Ir/CNT@TiO_2.

results demonstrate that introduction of CNT@TiO_2 nanocomposites support can be an effective way to improve activity and stability of Ir nanoparticle catalyst in the PEMWE anode.

4. Conclusion

In this study, we present CNT and TiO_2 nanocomposite (CNT@TiO_2) as a high-performance support for Ir nanoparticle catalyst toward the OER in the PEMWE anode. TiO_2 was synthesized in a form of thin layers first and then nanoparticles on acid-treated CNTs. CNT@TiO_2 nanocomposites show a high electrical conductivity value of 1.6 ± 0.2 S cm^{-1}, that is lower than that of CNT but comparable to that of carbon black. Through XPS analysis, it was demonstrated that TiO_2 in CNT@TiO_2 promotes the formation of OER-active Ir(III) species in Ir/CNT@TiO_2. The strong interaction between Ir and TiO_2 prevents loss of Ir nanoparticles during OER, improving stability of Ir/CNT@TiO_2. Ir/CNT@TiO_2 demonstrated superior OER activity and stability to Ir black, Ir/C and Ir/CNT. Thus, introduction of CNT@TiO_2 nanocomposites support can be an effective way to improve performance and durability of Ir nanoparticle catalyst in the PEMWE anode. In addition to the high-performing support material, a novel solution-based layer-by-layer coating method that mimics atomic layer deposition (ALD) is presented with advantages of easy control of TiO_2 loading amount, cost-effectiveness and scalability.

Conflicts of interest

There are no conflicts to declare.

References

1 S. Shiva Kumar and V. Himabindu, Hydrogen production by PEM water electrolysis – a review, *Mater. Sci. Energy Technol.*, 2019, **2**, 442–454.
2 M. Carmo, D. L. Fritz, J. Mergel and D. Stolten, A comprehensive review on PEM water electrolysis, *Int. J. Hydrogen Energy*, 2013, **38**, 4901–4934.
3 Z. Chen, X. Duan, W. Wei, S. Wang and B.-J. Ni, Electrocatalysts for acidic oxygen evolution reaction: achievements and perspectives, *Nano Energy*, 2020, **78**, 105392.
4 Y. Zhang, X. Zhu, G. Zhang, P. Shi and A.-L. Wang, Rational catalyst design for oxygen evolution under acidic conditions: strategies toward enhanced electrocatalytic performance, *J. Mater. Chem. A*, 2021, **9**, 5890–5914.
5 M.-C. Chuang and J.-a. A. Ho, Efficient electrocatalytic oxidation of water: minimization of catalyst loading by an electrostatic assembly of hydrous iridium oxide colloids, *RSC Adv.*, 2012, **2**, 4092–4096.
6 S. Sui, X. Wang, X. Zhou, Y. Su, S. Riffat and C.-j. Liu, A comprehensive review of Pt electrocatalysts for the oxygen reduction reaction: nanostructure, activity, mechanism and carbon support in PEM fuel cells, *J. Mater. Chem. A*, 2017, **5**, 1808–1825.
7 H.-S. Oh, H. N. Nong, D. Teschner, T. Reier, A. Bergmann, M. Gliech, J. Ferreira de Araújo, E. Willinger, R. Schloegl and P. Strasser, Electrochemical catalyst-support effects and their stabilizing role for IrOx nanoparticle catalysts during the oxygen evolution reaction (OER), *J. Am. Chem. Soc.*, 2016, **138**(38), 12552–12563.
8 X. Wang, M. Waje and Y. Yan, CNT-based electrodes with high efficiency for PEMFCs, *Electrochem. Solid-State Lett.*, 2004, **8**, A42.
9 R. Badam, M. Hara, H.-H. Huang and M. Yoshimura, Synthesis and electrochemical analysis of novel IrO_2 nanoparticle catalysts supported on carbon nanotube for oxygen evolution reaction, *Int. J. Hydrogen Energy*, 2018, **43**(39), 18095–18104.
10 X. Wen, L. Bai, M. Li and J. Guan, Ultrafine iridium oxide supported on carbon nanotubes for efficient catalysis of oxygen evolution and oxygen reduction reactions, *Mater. Today Energy*, 2018, **10**, 153–160.
11 T. Fujigaya, Y. Shi, J. Yang, H. Li, K. Ito and N. Nakashima, A highly efficient and durable carbon nanotube-based anode electrocatalyst for water electrolyzers, *J. Mater. Chem. A*, 2017, **5**, 10584–10590.

12 B. J. Landi, M. J. Ganter, C. D. Cress, R. A. DiLeo and R. P. Raffaelle, Carbon nanotubes for lithium ion batteries, *Energy Environ. Sci.*, 2009, **2**, 638–654.

13 X. Li, W.-X. Chen, J. Zhao, W. Xing and Z.-D. Xu, Microwave polyol synthesis of Pt/CNTs catalysts: effects of pH on particle size and electrocatalytic activity for methanol electrooxidization, *Carbon*, 2005, **43**, 2168–2174.

14 E. Oakton, D. Lebedev, M. Povia, D. F. Abbott, E. Fabbri, A. Fedorov, M. Nachtegaal, C. Copéret and T. J. Schmidt, IrO_2–TiO_2: A High-Surface-Area, Active, and Stable Electrocatalyst for the Oxygen Evolution Reaction, *ACS Catal.*, 2017, **7**, 2346–2352.

15 M. Yuan, Y. Zhu, L. Deng, R. Ming, A. Zhang, W. Li, B. Chai and Z. Ren, IrO_2–TiO_2 electrocatalysts for the hydrogen evolution reaction in acidic water electrolysis without activation, *New J. Chem.*, 2017, **41**(14), 6152–6159.

16 H. Lv, G. Zhang, C. Hao, C. Mi, W. Zhou, D. Yang, B. Li and C. Zhang, Activity of IrO_2 supported on tantalum-doped TiO_2 electrocatalyst for solid polymer electrolyte water electrolyzer, *RSC Adv.*, 2017, **7**, 40427–40436.

17 R. V. Genova-Koleva, F. Alcaide, G. Álvarez, P. L. Cabot, H.-J. Grande, M. V. Martínez-Huerta and O. Miguel, Supporting IrO_2 and $IrRuO_x$ nanoparticles on TiO_2 and Nb-doped TiO_2 nanotubes as electrocatalysts for the oxygen evolution reaction, *J. Energy Chem.*, 2019, **34**, 227–239.

18 S. Schlicht, P. Büttner and J. Bachmann, Highly Active Ir/TiO_2 Electrodes for the Oxygen Evolution Reaction Using Atomic Layer Deposition on Ordered Porous Substrates, *ACS Appl. Energy Mater.*, 2019, **2**, 2344–2349.

19 C. V. Pham, M. Bühler, J. Knöppel, M. Bierling, D. Seeberger, D. Escalera-López, K. J. J. Mayrhofer, S. Cherevko and S. Thiele, IrO_2 coated TiO_2 core–shell microparticles advance performance of low loading proton exchange membrane water electrolyzers, *Appl. Catal., B*, 2020, **269**, 118762.

20 X. Wang, X. Wan, X. Qin, C. Chen, X. Qian, Y. Guo, Q. Xu, W.-B. Cai, H. Yang and K. Jiang, Electronic Structure Modulation of RuO_2 by TiO_2 Enriched with Oxygen Vacancies to Boost Acidic O_2 Evolution, *ACS Catal.*, 2022, **12**, 9437–9445.

21 E. Oakton, D. Lebedev, A. Fedorov, F. Krumeich, J. Tillier, O. Sereda, T. J. Schmidt and C. Copéret, A simple one-pot Adams method route to conductive high surface area IrO_2–TiO_2 materials, *New J. Chem.*, 2016, **40**, 1834–1838.

22 P. Mazúr, J. Polonský, M. Paidar and K. Bouzek, Non-conductive TiO_2 as the anode catalyst support for PEM water electrolysis, *Int. J. Hydrogen Energy*, 2012, **37**, 12081–12088.

23 C. Spöri, J. T. H. Kwan, A. Bonakdarpour, D. P. Wilkinson and P. Strasser, The Stability Challenges of Oxygen Evolving Catalysts: Towards a Common Fundamental Understanding and Mitigation of Catalyst Degradation, *Angew. Chem., Int. Ed.*, 2017, **56**, 5994–6021.

24 C. Hao, H. Lv, Q. Zhao, B. Li, C. Zhang, C. Mi, Y. Song and J. Ma, Investigation of V-doped TiO_2 as an anodic catalyst support for SPE water electrolysis, *Int. J. Hydrogen Energy*, 2017, **42**, 9384–9395.

25 C. Hao, H. Lv, C. Mi, Y. Song and J. Ma, Investigation of Mesoporous Niobium-Doped TiO_2 as an Oxygen Evolution Catalyst Support in an SPE Water Electrolyzer, *ACS Sustainable Chem. Eng.*, 2016, **4**, 746–756.

26 G. C. da Silva, S. I. Venturini, S. Zhang, M. Löffler, C. Scheu, K. J. J. Mayrhofer, E. A. Ticianelli and S. Cherevko, Oxygen evolution reaction on tin oxides supported iridium catalysts: do we need dopants?, *ChemElectroChem*, 2020, **7**, 2330–2339.

27 C. Glynn and C. O'Dwyer, Solution Processable Metal Oxide Thin Film Deposition and Material Growth for Electronic and Photonic Devices, *Adv. Mater. Interfaces*, 2017, **4**, 1600610.

28 F. Bonet, V. Delmas, S. Grugeon, R. Herrera Urbina, P. Y. Silvert and K. Tekaia-Elhsissen, Synthesis of monodisperse Au, Pt, Pd, Ru and Ir nanoparticles in ethylene glycol, *Nanostruct. Mater.*, 1999, **11**, 1277–1284.

29 E.-J. Kim, J. Shin, J. Bak, S. J. Lee, K. h. Kim, D. Song, J. Roh, Y. Lee, H. Kim, K.-S. Lee and E. Cho, Stabilizing role of Mo in TiO_2-MoO_x supported Ir catalyst toward oxygen evolution reaction, *Appl. Catal., B*, 2021, **280**, 119433.

30 S.-T. Kang, J.-Y. Seo and S.-H. Park, The Characteristics of CNT/Cement Composites with Acid-Treated MWCNTs, *Adv. Mater. Sci. Eng.*, 2015, (2015), 308725.

31 D. F. Abbott, D. Lebedev, K. Waltar, M. Povia, M. Nachtegaal, E. Fabbri, C. Copéret and T. J. Schmidt, Iridium Oxide for the Oxygen Evolution Reaction: Correlation between Particle Size, Morphology, and the Surface Hydroxo Layer from *Operando* XAS, *Chem. Mater.*, 2016, **28**, 6591–6604.

32 C. Spöri, P. Briois, H. N. Nong, T. Reier, A. Billard, S. Kühl, D. Teschner and P. Strasser, Experimental Activity Descriptors for Iridium-Based Catalysts for the Electrochemical Oxygen Evolution Reaction (OER), *ACS Catal.*, 2019, 6653–6663.

33 V. Pfeifer, T. E. Jones, J. J. Velasco Velez, C. Massue, M. T. Greiner, R. Arrigo, D. Teschner, F. Girgsdies, M. Scherzer, J. Allan, M. Hashagen, G. Weinberg, S. Piccinin, M. Havecker, A. Knop-Gericke and R. Schlögl, The Electronic Structure of Iridium Oxide Electrodes Active in Water Splitting, *Phys. Chem. Chem. Phys.*, 2016, **18**, 2292.

34 F. Claudel, L. Dubau, G. Berthomé, L. Sola-Hernandez, C. Beauger, L. Piccolo and F. Maillard, Degradation Mechanisms of Oxygen Evolution Reaction Electrocatalysts: A Combined Identical-Location Transmission Electron Microscopy and X-ray Photoelectron Spectroscopy Study, *ACS Catal.*, 2019, **9**, 4688–4698.